BMC Genomics

RESEARCH

Open Access

Unraveling salt-responsive genes in *Suaeda salsa* through genomic and transcriptomic profiling across salinity gradients

Min Li[1,2], Xiangyu Zhou[3], Jiaxin Wu[2], Edward M. Golenberg[1], Dongxiao Zhu[3], Peimin He[2*] and Chuanzhu Fan[1*]

Abstract

Salinity severely limits global crop productivity, prompting a need to uncover plant salinity adaptation strategies. *Suaeda salsa* (L.) Pall., a halophyte thriving in saline habitats, offers a valuable model to dissect plant growth mechanisms under saline conditions. Although a chromosome-level reference genome of *S. salsa* was recently published, the corresponding gene annotation remained unavailable. Using the Helixer tool, we generated and released the first publicly available genome annotation for *S. salsa*, exhibiting high completeness with 92.80% (1,498) complete BUSCOs, thus providing an essential genomic resource. Using the *S. salsa* reference genome and annotation, we conducted RNA-seq-based transcriptomic profiling of plants subjected to 0, 200, and 400 mM NaCl for 30 days, respectively. We identified 462 significantly differentially expressed annotated genes across all treatments, with 11 key candidates consistently regulated. These genes are involved in key salinity response-related processes, including ion transport, osmotic adjustment, antioxidant defense, hormone signaling, transcriptional regulation, and genome plasticity. Enrichment analyses further supported their roles in ion homeostasis, redox regulation, and metabolic adjustment. This study provides new insights into the long-term salt tolerance mechanisms of *S. salsa* during normal development. The findings lay a foundation for future functional studies, comparative evolutionary analyses, and genetic improvement of salt-tolerant crops.

Keywords Genome annotation, Growth, Salinity, *Suaeda salsa*, Transcriptome

Introduction

Soil salinity is a critical global threat that severely restricts plant growth and agricultural productivity by disrupting osmotic and ion balance and impairing metabolic pathways, which can greatly reduce crop yields [1, 2]. Halophytes are specialized plants that thrive and complete their life cycle in saline soils or waters, often performing optimally under such conditions [3].

Suaeda salsa (L.) Pall. is a leaf-succulent annual halophyte widely distributed in saline habitats across Eurasia and cultivated as a seawater-irrigated vegetable in coastal China [4]. *Suaeda salsa* exhibits pronounced salt-adaptive traits, including leaf succulence, efficient vacuolar Na^+ sequestration, and sustained photosynthetic activity

*Correspondence:
Peimin He
pmhe@shou.edu.cn
Chuanzhu Fan
cfan@wayne.edu
[1]Department of Biological Sciences, Wayne State University, Detroit, MI 48202, USA
[2]College of Oceanography and Ecological Science, Shanghai Ocean University, Shanghai 201306, China
[3]Department of Computer Sciences, Wayne State University, Detroit, MI 48202, USA

under high salinity [5]. At the genomic level, *S. salsa* is a diploid species (2n = 18) with a chromosome-scale genome of approximately 445.10 Mb, providing an essential foundation for dissecting halophyte-specific mechanisms of salinity adaptation [6].

Physiological studies have demonstrated that normal growth of *S. salsa* under saline conditions relies on coordinated regulation of hormonal signaling, ion compartmentation, and osmotic balance [5, 7–9]. In particular, active sequestration of Na^+ into vacuoles, mediated by proton gradients generated by vacuolar H^+ pumps, enables cytosolic ion homeostasis while allowing inorganic ions to function as the dominant osmoticum [5]. In parallel, accumulation of compatible solutes such as proline and glycine betaine contributes to osmotic adjustment, although soluble sugars typically account for a relatively small fraction of the total osmotic potential in this species [8, 10].

At the molecular level, functional genomic studies have identified that salt-responsive genes in *S. salsa*, some of which confer enhanced salinity tolerance when heterologously expressed in *Arabidopsis thaliana*, include genes involved in lipid remodeling, water transport, osmolyte biosynthesis, and antioxidant defense, highlighting the complexity of halophytic stress adaptation [11]. Transcriptomic and metabolomic studies further reveal extensive metabolic reprogramming under salt stress, characterized by increased accumulation of protective metabolites such as glycine betaine, proline, and allantoin, alongside reductions in specific sugars and amino acids [6, 8, 12, 13]. Comparative analyses indicate that many halophytes of the family Chenopodiaceae (now classified within Amaranthaceae), such as *Suaeda maritima*, *Suaeda salsa*, *Atriplex nummularia*, and *Salicornia europaea*, predominantly rely on ion-based osmotic adjustment and efficient ion compartmentation, with organic osmolytes contributing only marginally to total osmotic potential, in contrast to glycophytes [10, 14–16].

Despite these advances, comprehensive integration of transcriptomic data with high-quality genome annotations in *S. salsa* has remained limited. Transcriptome profiling is essential for capturing dynamic regulatory responses to salinity, particularly for distinguishing long-term adaptive regulation from transient stress responses. However, the absence of a publicly available, high-quality genome annotation has limited the accurate mapping of expression changes to specific loci, thereby constraining mechanistic interpretation.

Although a chromosome-level reference genome of *S. salsa*, generated using high-fidelity long-read sequencing (approximately 44× HiFi coverage), has been published and is publicly accessible [17], a high-quality, publicly available genome annotation has been lacking. To address this gap, we generated the first publicly available genome annotation for *S. salsa* in General Feature Format version 3 (GFF3). The annotation has been deposited in the open-access repository Figshare, providing a valuable resource for halophyte genomics research. Using this *S. salsa* genome and annotation as references, we conducted RNA-seq-based transcriptomic analyses across multiple salinity treatments. This comprehensive annotation facilitated the identification of key biological pathways associated with salt tolerance and revealed widespread and significant changes in salt-responsive gene expression. Through these analyses, we identified 11 candidate genes that were consistently differentially regulated in response to salinity. Together, our results provide new insights into the transcriptional strategies underlying long-term salinity adaptation in a true halophyte and establish a robust genomic resource for future functional and comparative studies aimed at improving salt tolerance in crops.

Results

Sequencing data and read mapping statistics

A total of nine RNA-seq libraries from *S. salsa* were sequenced, generating between 43.9 and 50.8 million clean reads per sample (Table S1). Sequencing quality consistently was high across all libraries, with Q20 values exceeding 99% and Q30 values approximately 97%. The average GC content ranged from 42.48% to 42.69%, showing minimal variation among samples.

Cleaned RNA-seq reads were aligned to the reference genome, yielding an average mapped read length of approximately 148 bp per sample. Unique mapping rates ranged from 84.70% to 85.22%, while multi-mapped reads accounted for 7.27% to 7.88%. Unmapped reads due to short length remained stable between 7.10% and 7.47%. These mapping statistics indicate consistent sequencing performance across samples and reliable alignment to the reference genome (Table 1).

Genome and genome annotation

RNA-seq reads were aligned to the *S. salsa* reference genome obtained from the Genome Warehouse (GWH) of the National Genomics Data Center (NGDC) under accession GWHBQEE00000000 (BioProject: PRJCA006671; Biosample: SAMC461466). Gene structure prediction produced the first publicly accessible GFF3 genome annotation for *S. salsa* (https://doi.org/10.6084/m9.figshare.31445281). In total, 26,035 protein-coding genes were predicted, each represented by a single transcript model.

Assessment of annotation completeness identified 92.8% complete, 1.5% fragmented, and 5.6% missing BUSCOs out of 1,614 ortholog groups (Table 2). In addition, the consistently high unique mapping rates of RNA-seq reads across samples (84.70–85.22%) support the

Table 1 Mapping statistics for RNA-seq samples

Sample	Input Reads	Uniquely Mapped (%)	Multi Mapped (%)	Unmapped (Too Short) (%)	Avg. Mapped Length (bp)
SS1_1	49,808,246	85.02	7.71	7.17	147.74
SS1_2	47,966,750	84.92	7.81	7.16	148.05
SS1_3	47,136,114	84.96	7.82	7.11	147.76
SS2_1	44,925,770	85.17	7.42	7.28	147.85
SS2_2	50,334,162	85.02	7.38	7.47	147.97
SS2_3	46,266,814	85.22	7.27	7.38	147.98
SS3_1	49,608,826	84.7	7.84	7.34	147.58
SS3_2	43,959,582	84.79	7.88	7.21	148.87
SS3_3	50,813,238	85.04	7.75	7.1	148.17

Table 2 BUSCO assessment of Helixer-predicted protein sequences

Category	Number	Percentage (%)
Complete BUSCOs (C)	1,498	92.80%
Single-copy (S)	1,409	87.30%
Duplicated (D)	89	5.50%
Fragmented BUSCOs (F)	25	1.50%
Missing BUSCOs (M)	91	5.60%
Total BUSCO groups (n)	1,614	-

overall quality of the transcriptomic data and its compatibility with the annotated reference genome.

Principal component analysis of transcriptomic responses to salinity

Multivariate analyses were conducted to assess global transcriptional variation among samples. Principal component analysis (PCA) revealed clear separation of samples according to salinity treatment (Fig. 1A). The first two principal components explained 55.93% (PC1) and 26.07% (PC2) of the total variance.

Permutational multivariate analysis of variance showed that salinity treatment accounted for a significant proportion of expression variance (R^2 = 0.738, F = 8.4484, p = 0.007), with low intra-group dispersion (Table S2). Hierarchical clustering of the top 1,000 most variable genes further distinguished samples by treatment while maintaining close clustering among biological replicates (Fig. 1B). Pearson correlation analysis showed high correlations among replicates ($r > 0.94$, $p < 0.001$; Fig. 1C). Boxplots of variance-stabilized expression values demonstrated comparable global expression distributions across all samples (Fig. 1D).

Differentially expressed genes identification

Pairwise comparisons were conducted among plants exposed to 0 mM (SS1), 200 mM (SS2), and 400 mM (SS3). Between SS2 and SS1, 4,173 differentially expressed genes (DEGs) were identified, including 2,721 upregulated and 1,452 downregulated genes (Table S3). The SS3 vs. SS1 comparison yielded 3,101 DEGs (1,991 upregulated and 1,110 downregulated; Table S4). A total of 2,712 DEGs were detected between SS3 vs. SS2, consisting of 1,347 upregulated and 1,365 downregulated genes (Table S5).

To visualize the global expression pattern, the union DEGs from the SS2 vs. SS1 and SS3 vs. SS1 comparisons were examined. A total of 5,380 unique DEGs were obtained after removing duplicates. Heatmap visualization based on Variance-stabilized and z-score-normalized expression values showed distinct clustering of samples according to salinity levels (Fig. 2A), with SS2 and SS3 clearly separated from SS1. This global expression pattern highlights coordinated transcriptional reprogramming in response to increasing salinity and confirms the consistency of biological replicates within each treatment group.

A Venn diagram revealed 462 genes that were consistently differentially expressed across all three comparisons (Fig. 2B). To further characterize the functional landscape of these ubiquitous DEGs, protein sequences encoded by the 462 genes were subjected to functional annotation using the InterPro web platform. In total, 445 DEGs were successfully annotated, yielding 5,763 functional annotation entries, while 17 genes lacked detectable InterPro signatures (Table S6).

Gene Ontology (GO) terms derived from InterPro annotation indicated that the shared DEGs were predominantly associated with core molecular functions and regulatory processes. To summarize these functional features and reduce redundancy among closely related GO terms, treemap visualization was performed using REVIGO, displaying only GO terms annotated by more than 20 genes to enhance interpretability (Fig. 3A–C).

Within the Molecular Function category (Fig. 3C), the most represented GO terms included protein binding (GO:0005515, 215 genes), ATP binding (GO:0005524, 184 genes), and DNA binding (GO:0003677, 128 genes), reflecting extensive involvement of regulatory proteins, enzymes, and transcription-associated factors. Several catalytic and signaling-related functions were also prominent, including protein kinase activity (GO:0004672, 113

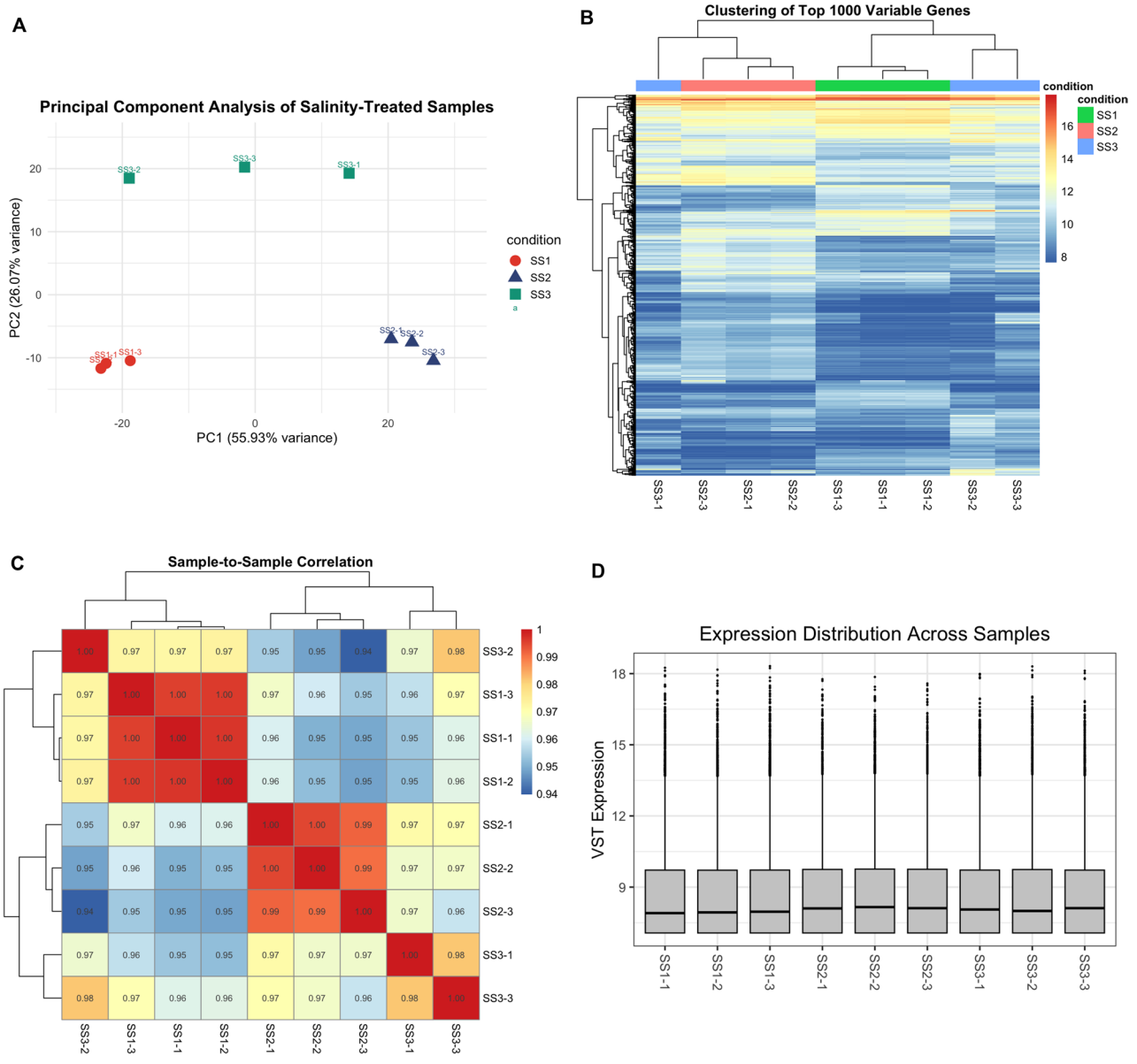

Fig. 1 Transcriptomic quality assessment of *S. salsa* samples under salinity treatments. **A** Principal component analysis (PCA) based on variance-stabilized expression values shows distinct clustering of SS1 (0 mM NaCl), SS2 (200 mM), and SS3 (400 mM) samples. **B** Heatmap of the top 1,000 most variable genes reveals consistent within-group clustering. **C** Sample-to-sample Pearson correlation matrix illustrates high reproducibility among replicates. **D** Boxplot of normalized gene expression across samples. PCA grouping was further supported by PERMANOVA ($R^2 = 0.738$, $p = 0.007$), as detailed in Supplementary Table S2

genes) and multiple oxidoreductase-related activities, such as heme binding (GO:0020037, 121 genes), monooxygenase activity (GO:0004497, 58 genes), and oxidoreductase activity acting on paired donors (GO:0016705, 62 genes).

In the Biological Process category (Fig. 3B), GO terms related to protein phosphorylation (GO:0006468, 125 genes), transcriptional regulation (GO:0003700 and GO:0006355, 57 genes each), and response to oxidative stress (GO:0006979, 63 genes) were highly represented, suggesting coordinated regulation of signaling pathways and stress-responsive processes under saline conditions. Enrichment of membrane-related components (GO:0016020, 53 genes) in the Cellular Component category (Fig. 3A) further highlights the importance of membrane-associated proteins in cellular adjustment to salinity.

To provide a global overview and statistical context for these functional patterns, conventional GO enrichment analysis was also performed on the 462 shared DEGs (Fig. 3D). Consistent with the InterPro-based annotation, enriched Biological Process terms included cellular

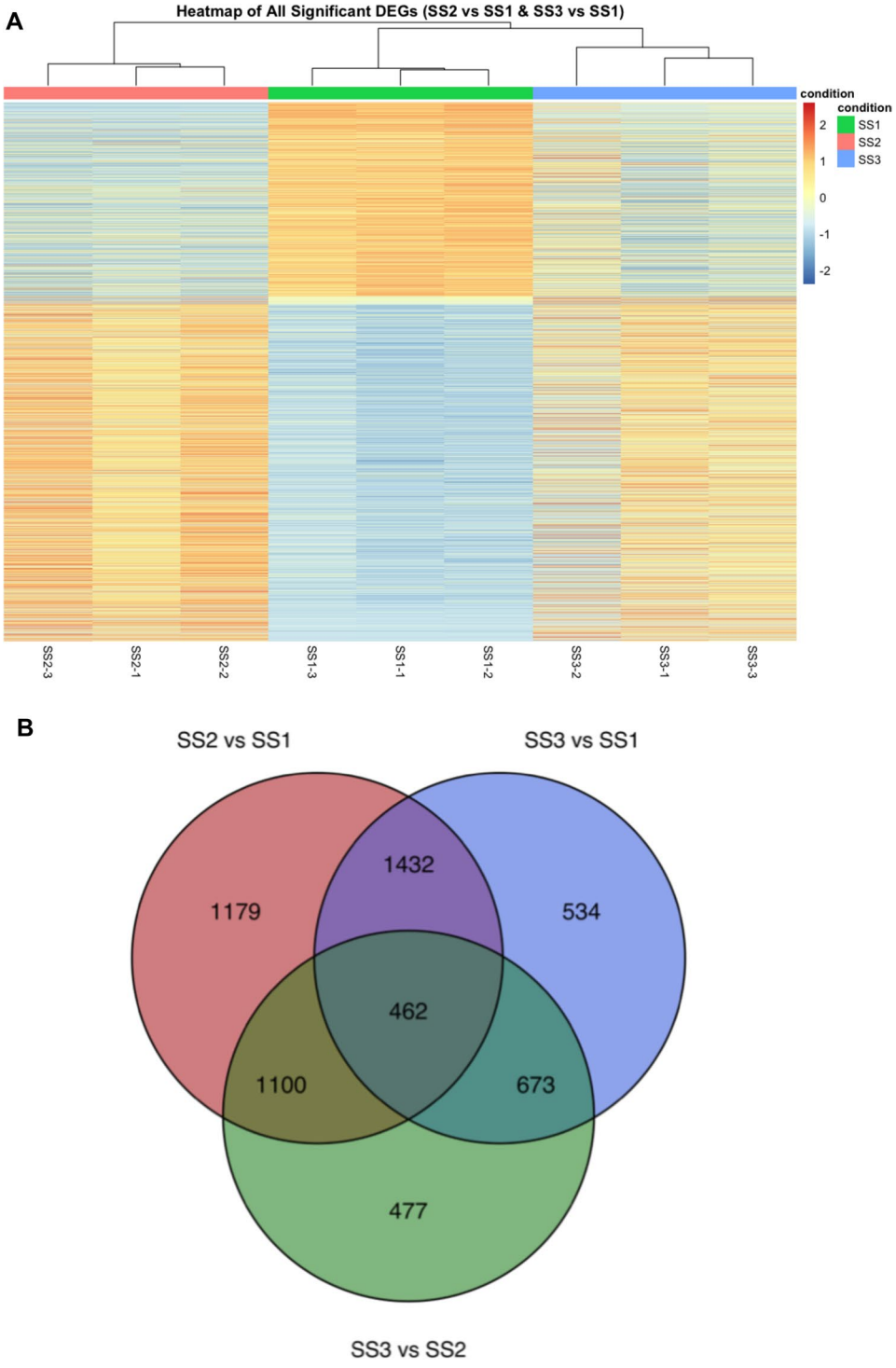

Fig. 2 Transcriptional response of *S. salsa* to salinity stress. **A** Heatmap of 5,380 unique differentially expressed genes (DEGs) identified from the union of SS2 vs. SS1 and SS3 vs. SS1 comparisons. Variance-stabilized and z-score normalized expression values are shown. Genes were ordered by average $\log_2$ fold change. Clustering reveals distinct transcriptional profiles across salinity treatments. **B** Venn diagram illustrating the overlap of DEGs among three salinity treatment comparisons (SS2 vs. SS1, SS3 vs. SS1, and SS3 vs. SS2) in *S. salsa*. A total of 462 DEGs were identified as common to all three comparisons

Fig. 3 Treemap visualization of major Gene Ontology (GO) functional categories among 462 DEGs under salinity treatments. Treemaps summarize selected GO terms associated with the 462 DEGs consistently detected across all salinity comparisons. **A** Cellular Component (CC), **B** Biological Process (BP), and **C** Molecular Function (MF) categories are shown separately. Only GO terms annotated by more than 20 genes were included, yielding 26 representative terms. Rectangle size reflects the number of annotated genes, and colors denote functionally related GO clusters summarized by REVIGO. **D** Gene Ontology (GO) enrichment analysis of the shared DEGs. The top 20 significantly enriched GO terms are shown, categorized into Biological Process, Cellular Component, and Molecular Function. Bar lengths indicate the number of genes associated with each GO term

process (GO:0009987), metabolic process (GO:0008152), and response to stimulus (GO:0050896). The Molecular Function category was dominated by catalytic activity (GO:0003824), while the Cellular Component category was enriched for membrane (GO:0016020), cytoplasm (GO:0005737), and related subcellular components.

Together, the concordant results from GO enrichment and InterPro-based functional annotation indicate that the ubiquitous DEGs are primarily involved in regulatory control, energy metabolism, redox balance, and signal transduction. These functional features provide a mechanistic framework for understanding the transcriptional programs underlying salinity adaptation and sustained growth in *S. salsa*.

Identification of key genes for *S. salsa* growth under saline conditions

To further elucidate transcriptional mechanisms supporting growth under saline conditions, the 462 ubiquitously DEGs were examined in detail. Based on consistent expression trends across increasing salinity levels and functional annotations, eleven genes were identified as key candidates potentially contributing to salinity tolerance and sustained growth in *S. salsa* ((Fig. 4; Table 3).

Among the genes upregulated under saline conditions, chr2_003131 (phosphoenolpyruvate carboxylase, PEPC) showed a robust stepwise increase in transcript abundance. Specifically, its expression was upregulated by 2.50-fold ($\log_2$FC = 1.32) in the SS2 vs. SS1 comparison and further increased by 3.76-fold ($\log_2$FC = 1.91) in the SS3 vs. SS2, resulting in an overall 9.4-fold induction ($\log_2$FC = 3.23) under high salinity (Table S7). As PEPC is a key enzyme involved in organic acid metabolism, its sustained upregulation suggests an important role in enhancing carbon fixation efficiency and maintaining cellular osmotic balance in saline environments.

Several additional genes were strongly induced, reflecting higher metabolic demands. chr6_000414.1 (Ribonuclease 1, RNS1) and chr8_000327.1 (Phosphoglycerate kinase, PGK) were upregulated by 12.8-fold ($\log_2$FC = 3.68) and 10.3-fold ($\log_2$FC = 3.36) in SS3 vs. SS1, respectively. Similarly, chr4_002858.1 (bZIP transcription factor FD) was consistently induced, reaching 6.7-fold ($\log_2$FC = 2.74) under high salinity. Additionally, chr3_000195.1 (probable serine/threonine-protein kinase PBL26) was identified as strictly salinity-inducible, shifting from undetectable in control conditions to high expression in SS3 (FC = 50.1; $\log_2$FC = 5.65), suggesting its specific role in rapid hypersaline adaptation.

Chr2_001401.1 (LTR copia-type retrotransposon) was activated under high salinity. Its expression increased 468-fold ($\log_2$FC = 8.87) from negligible in SS1 to extremely high in SS3. This dramatic transposon activation suggests salt stress may induce "genomic shock,"

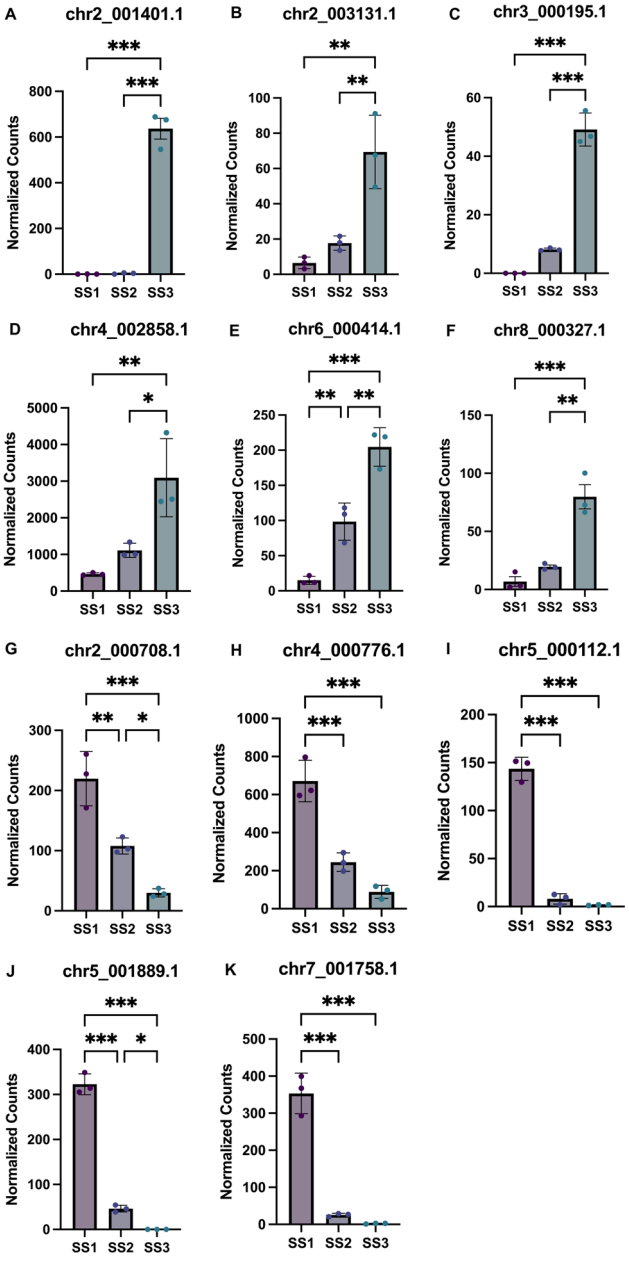

Fig. 4 Expression patterns of key salt-responsive genes in *S. salsa* under increasing salinity. **A–F** Six genes were significantly upregulated in response to increasing NaCl concentrations (0, 200, and 400 mmol/L). **G–K** Five genes were significantly downregulated under salinity stress. Gene expression values are shown as normalized counts (mean ± SEM, $n = 3$). Statistical significance was assessed using one-way ANOVA followed by multiple comparisons. Significant differences among treatment groups are indicated by asterisks: $p < 0.05$ (*), $p < 0.01$ (**), $p < 0.001$ (***). All upregulated genes show monotonic increases, while all downregulated genes exhibit consistent suppression under rising salinity conditions, indicating their potential regulatory roles in *S. salsa* salt stress adaptation

potentially driving genomic plasticity and transcriptional reprogramming as an adaptation.

Conversely, a subset of genes was strongly downregulated, indicating a shift in physiological priorities. chr7_001758.1 (chloroplastic cysteine synthase, CS) showed the most severe suppression, with expression levels dropping to near zero (FC = 0.01; $\log_2$FC = – 6.81) in SS3 vs. SS1. Genes associated with oxidative stress and carbohydrate biosynthesis were also markedly suppressed. For example, chr5_001889.1 (cytosolic ascorbate peroxidase, cAPX), and chr5_000112.1 (galactinol synthase), exhibited strong downregulation (FC = 0.03; $\log_2$FC = – 5.0). In addition, chr4_000776.1 (ethylene-responsive transcription factor ABR1) and the abscisic acid biosynthesis–related gene chr2_000708.1 (zeaxanthin epoxidase, ZEP) showed significant repression ($\log_2$FC = – 2.91 and – 2.83, respectively). Collectively, this coordinated downregulation suggests a strategic metabolic reprogramming, potentially aimed at conserving energy and reallocating resources toward pathways critical for long-term survival under high salinity.

Pathway enrichment and network analysis

KEGG pathway enrichment analysis was performed on the identified candidate genes. Seven genes were assigned KEGG Orthology identifiers, linking them to 20 metabolic pathways (Fig. 5). The resulting pathway-gene network highlighted pathways related to carbon metabolism, glycolysis/gluconeogenesis, glutathione metabolism, and sulfur metabolism. Several genes, including chr7_001758.1 (chloroplastic cysteine synthase), chr8_000327.1 (phosphoglycerate kinase), and chr2_003131.1 (phosphoenolpyruvate carboxylase), were associated with multiple pathways, indicating extensive pathway connectivity among the salinity-responsive genes.

Discussion

Salinity significantly restricts plant growth, development, and agricultural productivity, necessitating sophisticated physiological and molecular adaptations [18]. In this study, we comprehensively characterized the transcriptional landscape of normal growth *S. salsa* plants under incremental salinity conditions, leveraging the first publicly available genome annotation for this halophyte [6]. Our comprehensive transcriptomic RNA-seq analysis revealed extensive transcriptional reprogramming across a gradient of salinity, with 462 DEGs. Specifically, we identified 11 robust candidate genes that exhibited consistent trends (up- or down-regulation) with increasing salinity ($p < 0.05$, $\log_2|\text{Fold Change}| > 1$).

Several upregulated candidate genes are directly linked to metabolic and energetic processes critical for salt tolerance. The coordinated induction of phosphoenolpyruvate carboxylase (PEPC; chr2_003131.1) and phosphoglycerate kinase (PGK; chr8_000327.1) indicates sustained transcriptional reinforcement of central carbon metabolism in *S. salsa*. PEPC catalyzes an anaplerotic

Table 3 Functional annotation and PFAM domains of the 11 candidate genes under salt stress

Gene_ID	Description	PFAMs	Expression under salt stress
chr2_001401.1	gag-polypeptide of LTR copia-type	Retrotran_gag_2, Retrotran_gag_3, Retrotrans_gag, gag_pre-integrs, rve	up
chr2_003131.1	phosphoenolpyruvate carboxylase	PEPcase	up
chr3_000195.1	Probable serine/threonine-protein kinase PBL26	Pkinase, Pkinase_Tyr	up
chr4_002858.1	bZIP transcription factor FD	bZIP_1	up
chr6_000414.1	Ribonuclease 1 (RNS1)	Ribonuclease_T2	up
chr8_000327.1	Phosphoglycerate kinase	PGK	up
chr2_000708.1	Zeaxanthin epoxidase (ZEP)	FAD_binding_3, FHA, NAD_binding_8	down
chr4_000776.1	Ethylene-responsive transcription factor ABR1	AP2	down
chr5_000112.1	Raffinose synthase (RS)	Raffinose_syn	down
chr5_001889.1	Cytosolic ascorbate peroxidase (cAPX)	peroxidase	down
chr7_001758.1	Chloroplastic cysteine synthase (CS)	PALP	down

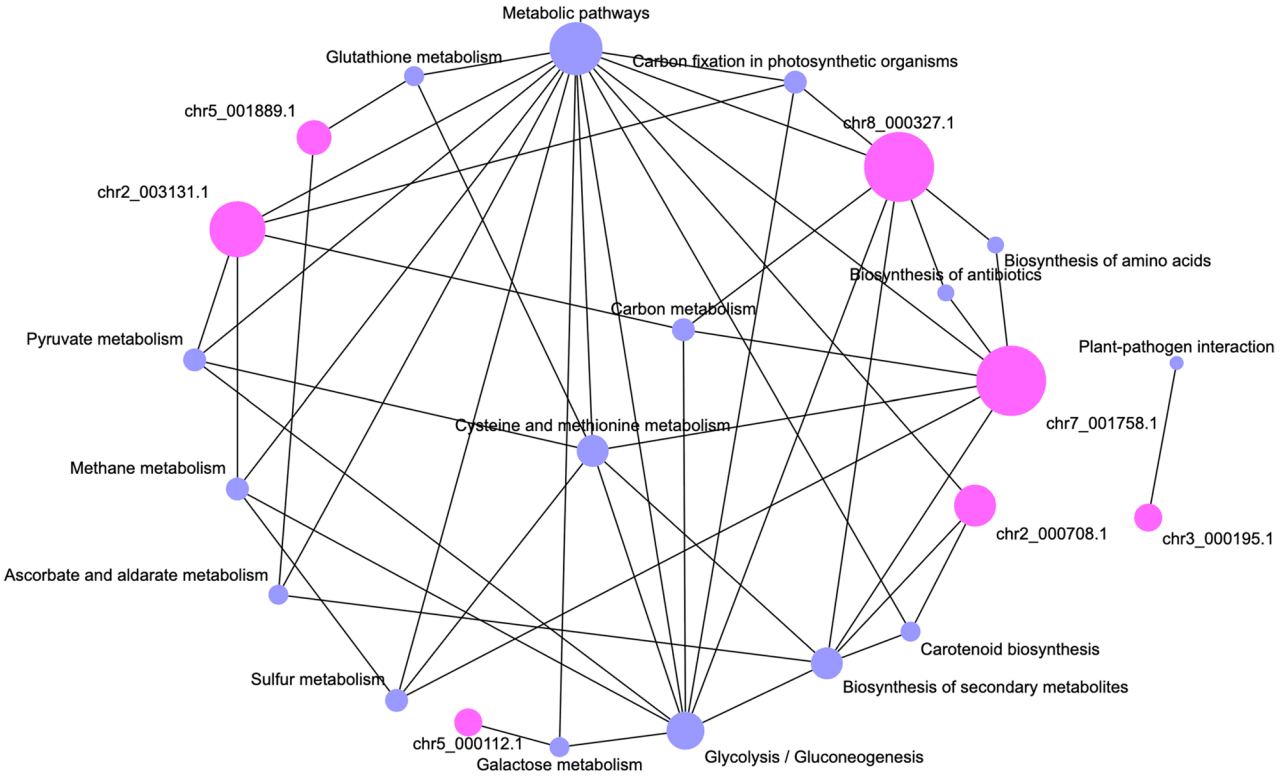

Fig. 5 KEGG pathway–gene network of selected differentially expressed genes. The network illustrates the associations between KEGG pathways (purple nodes) and input genes (pink nodes). Node size represents the number of connections (degree), and edges indicate known functional relationships based on KEGG pathway annotation. For pathway nodes, larger circle sizes indicate a higher number of associated DEGs

CO_2 fixation reaction, replenishing C_4-dicarboxylic acids and supporting organic acid metabolism, cellular pH buffering, and metabolic stability [19–21]. In parallel, PGK catalyzes an ATP-generating step in glycolysis, sustaining glycolytic flux and cellular energy supply [22], and has been associated with improved ion homeostasis and osmolyte accumulation under saline conditions [23]. Together, these responses suggest that metabolic reprogramming under salinity prioritizes energetic stability and osmotic homeostasis during prolonged stress.

In contrast, genes involved in compatible solute and sulfur metabolism, including raffinose synthase (RafS; chr5_000112.1) and chloroplastic cysteine synthase (CS; chr7_001758.1), were downregulated under salinity. While these pathways are commonly induced in glycophytes to support osmotic protection and glutathione-dependent redox homeostasis [24–30], their regulation is highly species- and context-dependent. As a euhalophyte, *S. salsa* primarily relies on inorganic ion–based osmotic adjustment, with Na^+ and Cl^- accounting for ~ 67% of

total osmotic solutes in Amaranthaceae species, whereas soluble sugars contribute only ~ 1% [5, 10, 15, 16]. This quantitative distinction provides a physiological basis for the attenuated induction of organic solute–related pathways in *S. salsa* under prolonged salinity.

The downregulation of cytosolic ascorbate peroxidase (cAPX; chr5_001889.1) represents a departure from the classical oxidative stress paradigm in glycophytes. Although cAPX detoxifies cytosolic H_2O_2 via the ascorbate–glutathione cycle [31], accumulating evidence indicates that ROS accumulation does not necessarily equate to cellular damage under abiotic stress [32, 33]. Recent studies highlight reactive carbonyl species (RCS) as dominant cytotoxic agents regulating stress-induced programmed cell death [34–36]. Consistent with this framework, tolerant halophytes exhibit a strategic tolerance to elevated ROS signaling, prioritizing the maintenance of essential H_2O_2 signaling while simultaneously enhancing RCS detoxification capacity via upregulated AO activity [37]. This suggesting that cAPX downregulation in *S. salsa* reflects a strategic reconfiguration of oxidative stress management by prioritizing the maintenance of ROS-mediated signaling over total elimination rather than compromised antioxidant defense.

Applying this paradigm to *S. salsa*, the observed downregulation of cAPX likely reflects a sophisticated reconfiguration of oxidative stress management rather than a compromised antioxidant defense. In this species, efficient vacuolar ion sequestration limits ionic imbalance–induced ROS generation at its source, thereby reducing the requirement for strong induction of NADPH-dependent ROS-scavenging pathways such as the ascorbate–glutathione cycle [10, 38]. Instead, *S. salsa* appears to prioritize tolerance mechanisms that mitigate downstream carbonyl toxicity while allowing controlled H_2O_2 signaling to operate within adaptive regulatory networks.

This reconfiguration is further supported by transcriptional signatures indicative of ROS avoidance and signaling optimization. The downregulation of zeaxanthin epoxidase (ZEP; chr2_000708.1) likely restricts the conversion of zeaxanthin to violaxanthin, promoting zeaxanthin accumulation and enhancing non-photochemical quenching (NPQ) [39–41]. By dissipating excess excitation energy as heat, this mechanism prevents excessive ROS formation at the photosynthetic source, thereby reducing the burden on cytosolic antioxidant systems such as cAPX [42, 43]. At the signaling level, the coordinated upregulation of the receptor-like cytoplasmic kinase PBL26 (chr3_000195.1) and downregulation of the AP2/ERF transcription factor ABR1 (chr4_000776.1), a known repressor of ABA signaling, suggest enhanced stress perception and signal amplification without the metabolic cost of extensive hormone biosynthesis [44, 45]. In parallel, the upregulation of ribonuclease RNS1 (chr6_000414.1) may facilitate nutrient remobilization, supporting ion transport and metabolic adjustment during prolonged salinity exposure [46, 47].

Under sustained salinity, *S. salsa* also exhibits signs of deeper transcriptional and genomic reprogramming. The strong induction of an LTR copia-type retrotransposon (chr2_001401.1) suggests activation of transposable elements, which may contribute to genomic plasticity by reshaping chromatin structure or modulating neighboring gene expression [48, 49]. Although the functional consequences of this activation remain unclear, it may reflect stress-induced relaxation of epigenetic repression or represent a trade-off associated with prolonged environmental pressure.

In summary, our findings reveal a temporally structured, multi-tiered adaptation strategy in *S. salsa* that integrates reinforcement of central metabolic, predominantly ion-dominated osmotic adjustment, reprogrammed oxidative stress management, and long-term transcriptional and genomic plasticity. Consistent with these gene-level responses, GO treemap and KEGG enrichment analyses indicate that ubiquitously salt-responsive genes are mainly involved in core metabolic processes, signal transduction, redox regulation, and membrane-related functions. This pattern indicates a coordinated systems-level optimization that supports sustained growth under salinity, rather than a generalized stress-induced response. Therefore, the candidate genes identified in this study provide valuable entry points for dissecting the mechanisms underlying halophyte resilience and represent promising resources for the genetic improvement of salinity tolerance in crop species. Although qRT-PCR validation was not performed in this study, our previous experiments have confirmed the reliability of our RNA-seq pipeline [50]. Future investigations combining spatiotemporal expression profiling, functional validation (e.g., CRISPR/Cas9-mediated mutagenesis and overexpression), targeted biochemical measurements of osmoprotectants, and epigenetic analyses will be essential to further elucidate the regulatory architecture governing long-term salinity adaptation in halophytic plants.

Materials and methods

Plant growth and sample collection

Suaeda salsa seeds were sourced from Suqian City, Jiangsu Province, China. Species identification was independently confirmed by Prof. Jingkuan Sun, a botanist and ecologist at Shandong University of Aeronautics, based on morphological characteristics according to the *Flora of China*. A voucher specimen was prepared during the study, and digital images of the specimen are retained by the research group at Shanghai Ocean University. After surface sterilization in 1% potassium permanganate

for 20 min, seeds were rinsed thoroughly and imbibed in water for 24 h. Seeds were then sown in perforated pots under controlled conditions (25 °C day/20°C night, 600 $\mu mol \cdot m^{-2} \cdot s^{-1}$ light intensity, 14 h light/10 h dark photoperiod) and irrigated daily with half-strength Hoagland nutrient solution containing 100 $mmol \cdot L^{-1}$ NaCl. The detailed composition of the nutrient solution is described in our previous work [50]. Seedlings of *S. salsa* were first germinated and grown under uniform, non-saline conditions until they developed six pairs of true leaves. At this stage, plants were assigned to three treatment groups designated as SS1, SS2, and SS3, corresponding to salinity levels of 0, 200, and 400 mM NaCl, respectively. The selected salinity concentrations are consistent with previous studies on *S. salsa*, where 200 mM NaCl [51] is considered an optimal growth condition, and 400 mM NaCl represents a higher salinity level used to investigate stress responses [52]. The salt treatments were maintained for 30 consecutive days. After 30 days of salinity treatment, leaf tissues from the upper third of each plant were harvested for RNA extraction and transcriptome sequencing. This prolonged salinity treatment was designed to capture transcriptional programs associated with long-term salinity adaptation during normal vegetative growth, rather than transient stress responses.

Source of genome and genome annotation

The reference genome of *S. salsa* used in this study was downloaded from the Genome Warehouse (GWH) of the National Genomics Data Center (NGDC) under accession GWHBQEE00000000 (BioProject: PRJCA006671; Biosample: SAMC461466). The chromosome-level genome assembly was originally generated by Wang et al. [17] using high-fidelity PacBio HiFi sequencing combined with Hi-C scaffolding.

As no official GFF annotation was available, gene annotation was performed by using a GFF3 file predicted by Helixer v0.3.4 [53]. This annotation was used for read summarization and gene-level quantification. The -g ID parameter was specified during count matrix generation to group transcript features by gene ID. To evaluate the completeness of the Helixer-derived gene annotation, BUSCO v5.8.2 [54] was run on the predicted protein sequences by using the *embryophyta_odb10* lineage dataset (2025-06-19).

Genome indexing was performed by using STAR v2.7.11b [55] with the genome FASTA file and the Helixer-generated GFF3 annotation. STAR indices were generated by using the parameters --sjdbOverhang 99 and --sjdbGTFtagExonParentTranscript Parent, which optimize spliced alignment for GFF3-formatted annotations [55].

RNA extraction, library construction, and high-throughput Illumina sequencing

Total RNA was extracted from tissue samples and sequenced by Majorbio Co., Ltd. (Shanghai, China) using TGuide S96 Magnetic Bead-based Polysaccharide & Polyphenol Plant Total RNA Extraction Kit (Tiangen Biotech Co., Ltd., China), following the manufacturer's instructions and standardized quality control procedures. Three biological replicates were included for each treatment. RNA quality was rigorously assessed by using multiple approaches: RNA concentration and purity were measured with a Nanodrop 2000 spectrophotometer, integrity was evaluated by agarose gel electrophoresis, and RNA Quality Number (RQN) was determined by using the Agilent 5300 Fragment Analyzer (Agilent Technologies, USA) with the DNF-471 RNA Kit, following the manufacturer's instructions. Only RNA samples meeting the following strict criteria were used for library construction: total RNA quantity ≥ 1 μg, concentration ≥ 30 ng/μL, RQN > 6.5, and an OD260/280 ratio between 1.8 and 2.2, following standard molecular biology guidelines for RNA purity assessment [56].

Polyadenylated mRNAs were isolated from total RNA by using oligo(dT)-conjugated magnetic beads, which selectively bind to the poly(A) tails of eukaryotic mRNAs. Strand-specific libraries were constructed using the Illumina® Stranded mRNA Prep, Ligation (Standard) kit (Illumina, USA) according to the manufacturer's protocol. The purified mRNA was then fragmented into ~300 bp fragments by using the fragmentation buffer under controlled conditions to suit short-read sequencing requirements. First-strand cDNA was synthesized by using random primers and reverse transcriptase, followed by second-strand synthesis to generate double-stranded cDNA. End-repair was then performed to produce blunt ends, and a single 'A' nucleotide was added to the 3′ ends to facilitate adapter ligation.

Adapter-ligated cDNA fragments were purified and size-selected, followed by PCR amplification to enrich for successfully ligated fragments. The final libraries were quantified by using a Qubit 4.0 fluorometer, pooled equimolar concentrations, and subjected to cluster generation by bridge PCR amplification on an Illumina cBot system. Paired-end sequencing (2 × 150 bp) was performed on an Illumina NovaSeq 6000 platform following the manufacturer's standard protocol.

RNA-seq data processing and gene expression quantification

Raw paired-end RNA-seq reads generated by the NovaSeq platform were first trimmed by using Cutadapt v4.9 [57] to remove Illumina universal adapter sequences (AG

ATCGGAAGAG) from both forward and reverse reads. Reads shorter than 25 bp after trimming were discarded. The quality of the trimmed reads was assessed by using FastQC v0.11.8 [58] to ensure sequencing integrity. For each sample, trimmed paired-end reads were concatenated before alignment.

Reads were aligned to the reference genome by using STAR with the options --outSAMstrandField intronMotif and --outSAMunmapped Within to retain splicing junctions and unmapped read information. The resulting SAM files were converted to BAM format, sorted, and indexed by using samtools v1.9 [59]. Gene-level quantification was performed by using featureCounts from the Subread package v2.0.6 [60], based on the Helixer-generated GFF3 annotation file. The resulting raw count matrix was used for downstream differential expression analysis by using the DESeq2 package [61] in R (v4.2.2).

RNA-seq quality control and multivariate statistical analysis

To assess the consistency and global structure of the RNA-seq dataset across treatments, we applied a series of multivariate analyses by using R. Variance-stabilizing transformation (VST), which was performed on raw count data by using DESeq2 [61]. And the transformed values were subsequently used for downstream visualization and statistical testing. Principal Component Analysis (PCA) was conducted by using the plotPCA() function from DESeq2 to reduce dimensionality and visualize sample clustering [61]. The top 500 most variable genes across all samples were included in the PCA calculation. The first two principal components (PC1 and PC2), which together explained > 80% of the variance, were plotted to illustrate inter- and intra-group sample separation.

To statistically validate the PCA-based groupings, we performed a permutational multivariate analysis of variance (PERMANOVA) by using the adonis2() function in the vegan package v2.6.10 [62].

Hierarchical clustering was conducted on the top 1,000 most variable genes by using Euclidean distance and complete linkage. This subset was selected to capture the major sources of transcriptional variation across samples while minimizing noise contributed by genes with low expression variance. Clustering results were visualized with a heatmap generated by using the pheatmap() function from the pheatmap package v1.0.12 [63], and both rows and columns were scaled to highlight variation across salinity treatments.

Sample-to-sample Pearson correlation analysis was performed by using the cor() function and hierarchical clustering to evaluate reproducibility among biological replicates. All pairwise correlation coefficients ($r > 0.94$) indicated high data quality. Statistical significance, assessed with the cor.test() function (based on the Fisher transformation), confirmed that all correlations were highly significant ($p < 0.001$).

Finally, expression distributions across all samples were visualized via boxplots of VST values by using base R functions, confirming that global gene expression levels were evenly distributed and free of batch effects.

Differential expression analysis and functional annotation

Downstream analyses were conducted in R contributed packages. Gene expression count matrices were filtered and processed by using DESeq2 [61]. The count values from three biological replicates under each condition (SS1, SS2, SS3) were combined and aggregated by gene ID. Redundant gene IDs were merged by summing their counts by using the summarise() function from dplyr v1.1.4. Differential gene expression analysis was performed by using DESeq2 with the model formula ~ condition. Genes were considered significantly differentially expressed if they met the thresholds of adjusted p.adj < 0.05 (two-tailed test) and $\log_2|\text{Fold Change}| > 1$.

To visualize global transcriptional patterns induced by salinity treatments relative to the control (0 mM NaCl), we compiled a union set of significantly DEGs from the SS2 vs. SS1 (200 mM vs. 0 mM) and SS3 vs. SS1 (400 mM vs. 0 mM) comparisons. This resulted in a total of 5,380 unique DEGs after removing overlapping genes. Variance-stabilized transformation (VST) was applied to the raw count matrix by using the vst() function in DESeq2 (with blind = FALSE) to normalize expression values and reduce heteroscedasticity [61]. The transformed expression matrix was then subset to include only the 5,380 DEGs.

To emphasize gene-level expression dynamics across treatments, we calculated the average $\log_2$ fold change for each gene across the two comparisons (SS2 vs. SS1 and SS3 vs. SS1) and used this metric to order genes from lowest to highest. Z-score normalization was applied row-wise to standardize expression values across samples for each gene. A heatmap was generated by using the pheatmap package [63], with hierarchical clustering applied to columns (samples) but not to rows (genes), thereby preserving the predefined gene order. Treatment conditions were annotated above the columns to reflect sample grouping by salinity level.

To understand their functions, we performed a comprehensive annotation analysis of these DEGs by using five databases: EggNOG mapper v2.1.12 [64], UniProt [65] (accessed April 2025), KEGG (accessed April 2025), RefSeq (accessed April 2025), and Gene Ontology. EggNOG mapper provided orthology-based functional assignments across multiple species. The output annotation file (out.emapper.annotations) was processed in R to extract Gene Ontology (GO) terms and KEGG ortholog (KO) identifiers for downstream functional annotation and pathway analyses.

GO enrichment analysis was conducted by using the enricher () function in the clusterProfiler package v4.12.6 [66]. GO terms were reformatted into a two-column TERM2GENE data frame, associating GO terms with corresponding gene IDs. For each contrast group (SS1 vs. SS2, SS1 vs. SS3, SS2 vs. SS3), significantly differentially expressed genes ($p < 0.05$ and $\log_2|\text{Fold Change}| > 1$) were used as input. Parameters were set to pvalueCutoff = 1, qvalueCutoff = 1, minGSSize = 1, and maxGSSize = 5000 to include all terms for exploratory visualization. Results were visualized by using the dotplot() function from enrichplot v1.24.4 [67]. KEGG pathway enrichment followed the same framework. KO identifiers were extracted and split by using the separate_rows() function from tidyr (v1.3.1), and a TERM2GENE data frame was constructed linking KO terms with gene IDs. KEGG enrichment was then performed by using the same statistical thresholds implemented in the clusterProfiler package [66].

To further characterize the functional features of the ubiquitously differentially expressed genes at the protein level, coding sequences corresponding to the 462 shared DEGs were translated into protein sequences and subjected to functional annotation using the InterPro web platform (InterProScan, EMBL-EBI). InterPro integrates multiple protein signature databases, including Pfam, SMART, PROSITE, SUPERFAMILY, and others, enabling comprehensive annotation of protein domains, families, and associated GO terms.

InterProScan annotation results were downloaded in tab-delimited format and processed in R. Proteins with at least one InterPro-derived GO term were retained for downstream analysis, while entries lacking functional signatures were recorded separately. For proteins annotated with multiple GO terms, all associated terms were retained to capture functional diversity.

All enrichment results were visualized as dot plots in R, and summary tables of enriched pathways were compiled for downstream interpretation. GO enrichment analysis was also conducted, and only the top 20 significantly enriched GO terms (ranked by p.adj) were included in the final figure. For KEGG enrichment results, circular bubble plots representing pathway enrichment statistics were generated by using the online platform OmicShare Tools [68]. In addition, GraphPad Prism version 10.4.2 (GraphPad Software, Inc.) was used to generate bar plots illustrating the expression patterns of selected DEGs across salinity gradients.

Conclusion

In summary, by integrating the *S. salsa* reference genome with newly generated genome annotations and transcriptome data, this study identified 11 consistently salt-responsive genes that collectively reflect central metabolic reinforcement, ion-dominated osmotic adjustment, reconfiguration of oxidative stress management, and regulatory plasticity characteristic of euhalophytes. These data resources and findings advance our understanding molecular mechanisms of plant growth under salinity conditions and provide a valuable foundation for future crop improvement efforts.

Abbreviations

AO	Aldehyde oxidase
BUSCO	Benchmarking Universal Single-Copy Orthologs
cAPX	Cytosolic ascorbate peroxidase
DEG	Differentially expressed gene
GO	Gene Ontology
KEGG	Kyoto Encyclopedia of Genes and Genomes
NCBI	National Center for Biotechnology Information
PCA	Principal component analysis
PEPC	Phosphoenolpyruvate carboxylase
PGK	Phosphoglycerate kinase
RCS	Reactive carbonyl species
RNS1	Ribonuclease 1
ROS	Reactive oxygen species
ZEP	Zeaxanthin epoxidase

Supplementary Information

The online version contains supplementary material available at https://doi.org/10.1186/s12864-026-12825-5.

Supplementary Material 1.

Supplementary Material 2.

Supplementary Material 3.

Supplementary Material 4.

Supplementary Material 5.

Supplementary Material 6.

Supplementary Material 7.

Acknowledgements

We thank Prof. Jingkuan Sun for assistance with species identification. We also thank the High Performance Computing (HPC) facilities at Wayne State University for providing computational resources and grid computing support.

Authors' contributions

ML: Writing - Original Draft, Conceptualization, Methodology, Validation, Investigation, Formal analysis. XZ: Software, Data Curation. JW: Writing - Original Draft. EG: Formal analysis, Writing - Review and Editing. DZ: Formal analysis, Data Curation, Writing - Review and Editing. PH: Conceptualization, Resources, Writing - Review and Editing, Funding acquisition. CF: Supervising, Data Curation, Conceptualization, Writing - Review and Editing.

Funding

This work was supported by the Open Fund of the Key Laboratory of Marine Ecological Monitoring and Restoration Technology of the Ministry of Natural Resources (MEMIRT202003) and Shanghai Lingang Coastal Marine Ecological Protection and Restoration Project (2201PD0001) to P.H.

Data availability

The original RNA-Seq datasets have been deposited in the NCBI Sequence Read Archive and are publicly available under the accession number PRJNA1227148. The genome annotation data have been deposited in the open-access repository Figshare and are publicly available at [https://doi.org/10.6084/m9.figshare.31445281].

Declarations

Ethics approval and consent to participate
Not applicable.

Consent for publication
Not applicable.

Competing interests
The authors declare no competing interests.

Received: 16 September 2025 / Accepted: 31 March 2026
Published online: 10 April 2026

References

1. Zhang X, Yao Y, Li X, Zhang L, Fan S. Transcriptomic analysis identifies novel genes and pathways for salt stress responses in *Suaeda salsa* leaves. Sci Rep. 2020;10:4236. https://doi.org/10.1038/s41598-020-61204-x.
2. Li T, Yang X, Sun H, Jing H, Bao S, Hu Y, et al. Competitive ion uptake and transcriptional regulation as a coordinated dual mechanism of NaCl-mediated cadmium detoxification in *Suaeda salsa*. Plant Physiol Biochem. 2025;224:109939. https://doi.org/10.1016/j.plaphy.2025.109939.
3. Munns R, Day DA, Fricke W, Watt M, Arsova B, Barkla BJ, et al. Energy costs of salt tolerance in crop plants. New Phytol. 2020;225:1072–90. https://doi.org/10.1111/nph.15864.
4. Mann A, Lata C, Kumar N, Kumar A, Kumar A, Sheoran P. Halophytes as new model plant species for salt tolerance strategies. Front Plant Sci. 2023;14. https://doi.org/10.3389/fpls.2023.1137211.
5. Song J, Wang B. Using euhalophytes to understand salt tolerance and to develop saline agriculture: *Suaeda salsa* as a promising model. Ann Botany. 2015;115:541–53. https://doi.org/10.1093/aob/mcu194.
6. Cui B, Liu R, Yu Q, Guo J, Du X, Chen Z, et al. Combined genome and transcriptome provides insight into the genetic evolution of an edible halophyte *Suaeda salsa* adaptation to high salinity. Mol Ecol. 2025;34:e17457. https://doi.org/10.1111/mec.17457.
7. Li W, Yamaguchi S, Khan MA, An P, Liu X, Tran L-SP. Roles of Gibberellins and Abscisic Acid in Regulating Germination of *Suaeda salsa* Dimorphic Seeds Under Salt Stress. Front Plant Sci. 2016;6. https://doi.org/10.3389/fpls.2015.01235.
8. Guo S-M, Tan Y, Chu H-J, Sun M-X, Xing J-C. Transcriptome sequencing revealed molecular mechanisms underlying tolerance of *Suaeda salsa* to saline stress. PLoS ONE. 2019;14:e0219979. https://doi.org/10.1371/journal.pone.0219979.
9. Seed germination and. seedling growth of *Suaeda salsa* under salt stress. Ann Botanici Fennici. 2007;44:161–9.
10. Flowers TJ, Colmer TD. Salinity tolerance in halophytes. New Phytol. 2008;179:945–63. https://doi.org/10.1111/j.1469-8137.2008.02531.x.
11. Sui N, Tian S, Wang W, Wang M, Fan H. Overexpression of Glycerol-3-Phosphate Acyltransferase from *Suaeda salsa* Improves Salt Tolerance in Arabidopsis. Front Plant Sci. 2017;8. https://doi.org/10.3389/fpls.2017.01337.
12. Wu H, Liu X, You L, Zhang L, Zhou D, Feng J, et al. Effects of Salinity on Metabolic Profiles, Gene Expressions, and Antioxidant Enzymes in Halophyte *Suaeda salsa*. J Plant Growth Regul. 2012;31. https://doi.org/10.1007/s00344-011-9244-6.
13. Yu W, Wu W, Zhang N, Wang L, Wang Y, Wang B, et al. Research Advances on Molecular Mechanism of Salt Tolerance in *Suaeda*. Biology. 2022;11:1273. https://doi.org/10.3390/biology11091273.
14. Munns R, Tester M. Mechanisms of salinity tolerance. Annu Rev Plant Biol. 2008;59:651–81. https://doi.org/10.1146/annurev.arplant.59.032607.092911.
15. Albert R, Pfundner G, Hertenberger G, Kastenbauer T, Watzka M. The physiotype approach to understanding halophytes and xerophytes. Ergebnisse weltweiter ökologischer Forschung. Stuttgart: Verlag Günter Heimbach; 2000. pp. 69–87.
16. Aronson J. HALOPH Salt Tolerant Plants for the World—A Computerized Global Data Base of Halophytes with Emphasis on Their Economic Uses. University of Arizona Press, Tucson. - References - Scientific Research Publishing. 1989. https://www.scirp.org/reference/referencespapers?referenceid=1480492. Accessed 2 Jan 2026.
17. Wang X, Xia J-B, Bai J-H, Yin S, Wang W, Wang D-W, et al. Multi-omics provides insights into genome evolution and betacyanin biosynthesis in the halophyte *Suaeda salsa*. J Syst Evol. 2024;62:1150–64. https://doi.org/10.1111/jse.13064.
18. Li H, Wang H, Wen W, Yang G. The antioxidant system in *Suaeda salsa* under salt stress. Plant Signal Behav. 2020;15:1771939. https://doi.org/10.1080/15592324.2020.1771939.
19. Izui K, Matsumura H, Furumoto T, Kai Y Phosphoenolpyruvate Carboxylase: a New Era of Structural Biology. Ann Rev Plant Biol. 2004;552004:69–84. . https://doi.org/10.1146/annurev.arplant.55.031903.141619.
20. Sánchez R, Flores A, Cejudo FJ. Arabidopsis phosphoenolpyruvate carboxylase genes encode immunologically unrelated polypeptides and are differentially expressed in response to drought and salt stress. Planta. 2006;223:901–9. https://doi.org/10.1007/s00425-005-0144-5.
21. de la Osa C, Pérez-López J, Feria A-B, Baena G, Marino D, Coleto I, et al. Knockdown of phosphoenolpyruvate carboxylase 3 negatively impacts growth, productivity, and responses to salt stress in sorghum (*Sorghum bicolor* L). Plant J. 2022;111:231–49. https://doi.org/10.1111/tpj.15789.
22. Chiarelli LR, Morera SM, Bianchi P, Fermo E, Zanella A, Galizzi A, et al. Molecular Insights on Pathogenic Effects of Mutations Causing Phosphoglycerate Kinase Deficiency. PLoS ONE. 2012;7:e32065. https://doi.org/10.1371/journal.pone.0032065.
23. Joshi R, Karan R, Singla-Pareek SL, Pareek A. Ectopic expression of Pokkali phosphoglycerate kinase-2 (OsPGK2-P) improves yield in tobacco plants under salinity stress. Plant Cell Rep. 2016;35:27–41. https://doi.org/10.1007/s00299-015-1864-z.
24. ElSayed AI, Rafudeen MS, Golldack D. Physiological aspects of raffinose family oligosaccharides in plants: protection against abiotic stress. Plant Biol. 2014;16:1–8. https://doi.org/10.1111/plb.12053.
25. Nishizawa A, Yabuta Y, Shigeoka S. Galactinol and raffinose constitute a novel function to protect plants from oxidative damage. Plant Physiol. 2008;147:1251–63. https://doi.org/10.1104/pp.108.122465.
26. Wirtz M, Droux M. Synthesis of the sulfur amino acids: cysteine and methionine. Photosynth Res. 2005;86:345–62. https://doi.org/10.1007/s11120-005-8810-9.
27. Hell R, Wirtz M. Molecular Biology, Biochemistry and Cellular Physiology of Cysteine Metabolism in *Arabidopsis thaliana*. Arabidopsis Book. 2011;9:e0154. https://doi.org/10.1199/tab.0154.
28. Li Z, Cheng L, Li S, Liu G, Liu S, Xu D, et al. Physiological, ionomic, transcriptomic and metabolomic analyses reveal molecular mechanisms of root adaption to salt stress in water spinach. BMC Genomics. 2025;26:231. https://doi.org/10.1186/s12864-025-11409-z.
29. Cui R, Wang X, Malik WA, Lu X, Chen X, Wang D, et al. Genome-wide identification and expression analysis of Raffinose synthetase family in cotton. BMC Bioinformatics. 2021;22:356. https://doi.org/10.1186/s12859-021-04276-4.
30. Egert A, Keller F, Peters S. Abiotic stress-induced accumulation of raffinose in Arabidopsis leaves is mediated by a single raffinose synthase (RS5, At5g40390). BMC Plant Biol. 2013;13:218. https://doi.org/10.1186/1471-2229-13-218.
31. Choudhury FK, Rivero RM, Blumwald E, Mittler R. Reactive oxygen species, abiotic stress and stress combination. Plant J. 2017;90:856–67. https://doi.org/10.1111/tpj.13299.
32. Mittler R. ROS Are Good. Trends Plant Sci. 2017;22:11–9. https://doi.org/10.1016/j.tplants.2016.08.002.
33. Xu L, Liu H, Mittler R, Shabala S. Useful or merely convenient: can enzymatic antioxidant activity be used as a proxy for abiotic stress tolerance? J Exp Bot. 2025;76:1524–33. https://doi.org/10.1093/jxb/erae524.
34. Liang X, Qian R, Ou Y, Wang D, Lin X, Sun C. Lipid peroxide-derived short-chain aldehydes promote programmed cell death in wheat roots under aluminum stress. J Hazard Mater. 2023;443:130142. https://doi.org/10.1016/j.jhazmat.2022.130142.
35. Biswas MS, Mano J. Reactive Carbonyl Species Activate Caspase-3-Like Protease to Initiate Programmed Cell Death in Plants. Plant Cell Physiol. 2016;57:1432–42. https://doi.org/10.1093/pcp/pcw053.
36. Ksas B, Chiarenza S, Dubourg N, Ménard V, Gilbin R, Havaux M. Plant acclimation to ionising radiation requires activation of a detoxification pathway against carbonyl-containing lipid oxidation products. Plant Cell Environ. 2024;47:3882–98. https://doi.org/10.1111/pce.14994.
37. Patel J, Khatri K, Sisay TA, Nja ZD, Choudhary B, Nurbekova Z, et al. UV-C-induced reactive carbonyl species are better detoxified in the halophytic plants *Salicornia brachiata* and *Arthrocnemum macrostachyum* than in the halophytic *Sarcocornia fruticosa* plants. Plant J. 2025;122:e70239. https://doi.org/10.1111/tpj.70239.

38. Bose J, Rodrigo-Moreno A, Shabala S. ROS homeostasis in halophytes in the context of salinity stress tolerance. J Exp Bot. 2014;65:1241–57. https://doi.org/10.1093/jxb/ert430.
39. Niyogi KK. Photoprotection revisited: Genetic and Molecular Approaches. Annu Rev Plant Physiol Plant Mol Biol. 1999;50:333–59. https://doi.org/10.1146/annurev.arplant.50.1.333
40. Demmig-Adams B, Adams WW. The role of xanthophyll cycle carotenoids in the protection of photosynthesis. Trends Plant Sci. 1996;1:21–6. https://doi.org/10.1016/S1360-1385(96)80019-7.
41. Havaux M, Niyogi KK. The violaxanthin cycle protects plants from photooxidative damage by more than one mechanism. Proc Natl Acad Sci. 1999;96:8762–7. https://doi.org/10.1073/pnas.96.15.8762.
42. Niyogi KK, Li X-P, Rosenberg V, Jung H-S. Is PsbS the site of non-photochemical quenching in photosynthesis? J Exp Bot. 2005;56:375–82. https://doi.org/10.1093/jxb/eri056.
43. Müller P, Li XP, Niyogi KK. Non-photochemical quenching. A response to excess light energy. Plant Physiol. 2001;125:1558–66. https://doi.org/10.1104/pp.125.4.1558.
44. Pandey GK, Grant JJ, Cheong YH, Kim BG, Li L, Luan S. ABR1, an APETALA2-Domain Transcription Factor That Functions as a Repressor of ABA Response in Arabidopsis. Plant Physiol. 2005;139:1185–93. https://doi.org/10.1104/pp.105.066324.
45. Lu D, Wu S, Gao X, Zhang Y, Shan L, He P. A receptor-like cytoplasmic kinase, BIK1, associates with a flagellin receptor complex to initiate plant innate immunity. Proc Natl Acad Sci. 2010;107:496–501. https://doi.org/10.1073/pnas.0909705107.
46. Bariola PA, Howard CJ, Taylor CB, Verburg MT, Jaglan VD, Green PJ. The Arabidopsis ribonuclease gene RNS1 is tightly controlled in response to phosphate limitation. Plant J. 1994;6:673–85. https://doi.org/10.1046/j.1365-313x.1994.6050673.x.
47. Velasco VME, Mansbridge J, Bremner S, Carruthers K, Summers PS, Sung WWL, et al. Acclimation of the crucifer Eutrema salsugineum to phosphate limitation is associated with constitutively high expression of phosphate-starvation genes. Plant Cell Environ. 2016;39:1818–34. https://doi.org/10.1111/pce.12750.
48. Makarevitch I, Waters AJ, West PT, Stitzer M, Hirsch CN, Ross-Ibarra J, et al. Transposable Elements Contribute to Activation of Maize Genes in Response to Abiotic Stress. PLoS Genet. 2015;11:e1004915. https://doi.org/10.1371/journal.pgen.1004915.
49. Jiao Y, Deng XW. A genome-wide transcriptional activity survey of rice transposable element-related genes. Genome Biol. 2007;8:R28. https://doi.org/10.1186/gb-2007-8-2-r28.
50. Cai L, Li M, Shen Y, Jiang R, Wang J, Ma S, et al. Betacyanin accumulation mediates photosynthetic protection in *Suaeda salsa* (L.) Pall. under salt stress. Planta. 2025;261:100. https://doi.org/10.1007/s00425-025-04664-7.
51. Song J, Wang B. Using euhalophytes to understand salt tolerance and to develop saline agriculture: *Suaeda salsa* as a promising model. Ann Bot. 2015;115:541–53. https://doi.org/10.1093/aob/mcu194.
52. Guo J, Du M, Tian H, Wang B. Exposure to High Salinity During Seed Development Markedly Enhances Seedling Emergence and Fitness of the Progeny of the Extreme Halophyte *Suaeda salsa*. Front Plant Sci. 2020;11:1291. https://doi.org/10.3389/fpls.2020.01291.
53. Stiehler F, Steinborn M, Scholz S, Dey D, Weber APM, Denton AK. Helixer: cross-species gene annotation of large eukaryotic genomes using deep learning. Bioinformatics. 2021;36:5291–8. https://doi.org/10.1093/bioinformatics/btaa1044.
54. Manni M, Berkeley MR, Seppey M, Simão FA, Zdobnov EM. BUSCO Update: Novel and Streamlined Workflows along with Broader and Deeper Phylogenetic Coverage for Scoring of Eukaryotic, Prokaryotic, and Viral Genomes. Mol Biol Evol. 2021;38:4647–54. https://doi.org/10.1093/molbev/msab199.
55. Dobin A, Davis CA, Schlesinger F, Drenkow J, Zaleski C, Jha S, et al. STAR: ultrafast universal RNA-seq aligner. Bioinformatics. 2013;29:15–21. https://doi.org/10.1093/bioinformatics/bts635.
56. NanoDrop 2000/2000c Spectrophotometers - User Manual. https://documents.thermofisher.com/TFS-Assets/CAD/manuals/NanoDrop-2000-User-Manual-EN.pdf.
57. Martin M. Cutadapt removes adapter sequences from high-throughput sequencing reads. EMBnet J. 2011;17:10–2. https://doi.org/10.14806/ej.17.1.200.
58. Andrews S. FastQC A Quality Control Tool for High Throughput Sequence Data. - References - Scientific Research Publishing. 2010. https://www.scirp.org/reference/referencespapers?referenceid=4024153. Accessed 30 Dec 2025.
59. Li H, Handsaker B, Wysoker A, Fennell T, Ruan J, Homer N, et al. The Sequence Alignment/Map format and SAMtools. Bioinformatics. 2009;25:2078–9. https://doi.org/10.1093/bioinformatics/btp352.
60. Liao Y, Smyth GK, Shi W. featureCounts: an efficient general purpose program for assigning sequence reads to genomic features. Bioinformatics. 2014;30:923–30. https://doi.org/10.1093/bioinformatics/btt656.
61. Love MI, Huber W, Anders S. Moderated estimation of fold change and dispersion for RNA-seq data with DESeq2. Genome Biol. 2014;15:550. https://doi.org/10.1186/s13059-014-0550-8.
62. Oksanen J, Simpson G, Blanchet FG, Kindt R, Legendre P, Minchin P, et al. Vegan community ecology package version 2.6-2 April 2022. 2022.
63. Kolde R, pheatmap. Pretty Heatmaps. 2010;1.0.13. https://doi.org/10.32614/CRAN.package.pheatmap.
64. Cantalapiedra CP, Hernández-Plaza A, Letunic I, Bork P, Huerta-Cepas J. eggNOG-mapper v2: Functional Annotation, Orthology Assignments, and Domain Prediction at the Metagenomic Scale. Mol Biol Evol. 2021;38:5825–9. https://doi.org/10.1093/molbev/msab293.
65. Coudert E, Gehant S, de Castro E, Pozzato M, Baratin D, Neto T, et al. Annotation of biologically relevant ligands in UniProtKB using ChEBI. Bioinformatics. 2022;39:btac793. https://doi.org/10.1093/bioinformatics/btac793.
66. Yu G, Wang LG, Han Y, He QY. clusterProfiler: an R package for comparing biological themes among gene clusters. OMICS. 2012;16:284–7. https://doi.org/10.1089/omi.2011.0118.
67. Yu G. enrichplot: Visualization of Functional Enrichment Result. https://bioconductor.org/packages/release/bioc/html/enrichplot.html.
68. Mu H, Chen J, Huang W, Huang G, Deng M, Hong S, et al. OmicShare tools: A zero-code interactive online platform for biological data analysis and visualization. Imeta. 2024;3:e228. https://doi.org/10.1002/imt2.228.

Publisher's note